DOI: 10.1002/chem.200600549

Gastrodin Interaction with Human Fibrinogen: Anticoagulant Effects and Binding Studies

Yang Liu,*[a, b] Xiaoling Tang,[c] Jianfeng Pei,[a] Li Zhang,[a] Feng Liu,[a] and Ke′an Li*[a]

Abstract: In an effort to identify the anticoagulant activity of gastrodin (GAS) and to investigate the possibility of its use as a novel anticoagulant drug, the binding characteristics of GAS to human fibrinogen (Fg) were studied by using a quartz crystal microbalance (QCM) biosensor, anticoagulant animal experiments, and a molecular docking simulation. Real-time kinetic analysis with the QCM biosensor revealed that the in vitro binding of GAS to Fg was strong under physiological ionic conditions as the determined equilibrium dissociation constant (K_D) was 1.94×10^{-6} M. To check whether this strong binding may influence the natural coagulation function of Fg, the in vivo effect of GAS on the coagulation system of rats was examined. The results showed that GAS can significantly prolong the coagulation time (CT) and decrease the Fg content, while it had no effect on the activated kaolin partial thromboplastin time (KPTT) or prothrombin time (PT) in rats. To clarify the mechanism of the specific interaction, a molecular docking simulation was also performed to provide reasonable binding models for the interaction of GAS with Fg at the atomic level. GAS binds strongly to the inherent polymerization sites "a" and "b" (holes) on the Fg molecule with similar binding free energies of about -34 kJ mol^{-1}. Altogether, these findings confirmed first that GAS possesses anticoagulant activity and that the possible anticoagulation mechanism of GAS mainly involves its interference with the knob-to-hole interactions between fibrin molecules, thereby effectively inhibiting the formation of clots and decreasing the risk of thrombosis. The study has also shown the potential usefulness of QCM biosensor technology for the rapid screening of drug–protein interactions.

Keywords: anticoagulant activity · biosensors · gastrodin · human fibrinogen · protein binding · proteins

Introduction

Protein binding is important in many processes that determine the eventual activity and fate of a drug once it has entered the body. A drug must interact with a biological target molecule, most often a protein, to exert a physiological function. Conversely, protein function is almost invariably linked with the specific binding of substrates or endogenous ligands.[1] Given the importance of these recognition events at the molecular level, a thorough understanding of the molecular forces that govern the affinities and specificities of drugs towards their macromolecular targets will contribute to the elucidation of the action mechanisms of drugs and the structure–activity relationships of proteins. The characterization of parameters for in vitro and in vivo drug binding to proteins is essential and this is particularly true in the design and development of new therapeutic agents.[2,3]

The plasma protein fibrinogen (Fg) is a 340 kDa dimeric glycoprotein that functions as the major structural clotting agent. It is composed of two copies of three nonidentical polypeptide chains, Aα, Bβ, and γ.[4,5] In the final stages of the blood coagulant cascade, Fg is transformed into an insoluble fibrin clot by the action of thrombin. The process is triggered by thrombin cleavage of fibrinopeptides A and B (FpA, FpB) from the amino termini of the Aα and Bβ chains in the E region, respectively. The removal of FpA exposes polymerization site "A" (Gly-Pro-Arg-Pro sequence),

[a] Dr. Y. Liu, Dr. J. Pei, Dr. L. Zhang, Prof. F. Liu, Prof. K. Li
College of Chemistry and Molecular Engineering
Peking University
Beijing, 100871 (China)
Fax: (+86) 10-6275-1708
E-mail: liuyang@gsu.edu
likean@dean.pku.edu.cn

[b] Dr. Y. Liu
Department of Chemistry, Georgia State University
Atlanta, GA, 30302-4098 (USA)
Fax: (+1) 404-651-2751

[c] Dr. X. Tang
Department of Pathology and Laboratory Medicine
Emory University School of Medicine
Atlanta, GA, 30322 (USA)

 © 2006 Wiley-VCH Verlag GmbH & Co. KGaA, Weinheim

Pagination corrected Oct. 17, 2006

while FpB removal uncovers polymerization site "B" (Gly-His-Arg-Pro sequence).[6] The newly formed "A" and "B" polymerization sites (knobs) in the E region of one fibrin molecule may interact with inherent polymerization sites "a" and "b" (holes) located in the γ and Bβ chains in the D region of another fibrin molecule. The noncovalent knob-to-hole interaction between one E region and two D regions of individual molecules (DD–E interaction) generates two stranded protofibrils in which individual monomers are half staggered with their D regions aligned in an end-to-end manner. The protofibrils associate with each other laterally to produce thicker fibrils that branch to form the fibrin clot.[7] Besides its prominent role in hemostasis, such a clot also increases the risk of thrombus formation.[8] Vascular thrombosis is the pathological hallmark of clinical syndromes such as myocardial infarction and stroke.[9] In the search for treatments for thrombotic disorders, much effort has been expended towards the development of inhibitors of the coagulant cascade. Based on the above coagulant mechanism, it is apparent that the inhibition of thrombin[10] or the interference of knob-to-hole interactions[11] will inhibit the formation of fibrin clots effectively, and thereby is essential for life.

Gastrodin (GAS), the main active ingredient of the Chinese herb "Tianma", is considered to have several beneficial properties, for example, improvement of circulation, treatment of headaches and vertigo, and anticonvulsant action.[12] People are becoming increasingly interested in GAS owing to its low toxicity and good therapeutic performance. Detailed characterization of the kinetics of GAS binding to proteins and definition of the binding sites on proteins will no doubt lead to a deeper understanding of the action mechanism of GAS at the molecular level. However, recent studies on GAS have focussed mainly on the identification and quantification of this active ingredient.[13,14] To the best of our knowledge, there is to date no report concerning the investigation of specific interactions between GAS and proteins.

In this study, a quartz crystal microbalance flow injection analysis (QCM-FIA) system with kinetic analysis software based on a genetic algorithm (GA)[15] was used for rapid screen analysis of the interactions between immobilized GAS and various proteins in solution. It was found for the first time that a strong specific interaction between GAS and Fg can occur under physiological ionic conditions. Since Fg plays an important role in the coagulant cascade, the strong binding of GAS may influence its natural coagulation function. To test this hypothesis, the in vivo effect of GAS on the coagulant system of rats was further investigated and classical coagulation tests, such as coagulation time (CT), Fg content, activated kaolin partial thromboplastin time (KPTT), and prothrombin time (PT), were performed. It was confirmed first that GAS possesses anticoagulant activity that was not related to intrinsic and extrinsic coagulation factors, mainly due to the strong binding of GAS to Fg. To gain a better understanding of the molecular basis for the interaction, a molecular docking method was also used to provide reasonable and reliable binding models and to define the binding sites on Fg. A possible anticoagulant mechanism for GAS has been proposed.

Results and Discussion

QCM biosensor analysis: A wide variety of biochemical techniques (ultrafiltration, ultracentrifugation, and equilibrium dialysis) have been extensively employed in the study of drug–protein binding.[16] These techniques are based on the analysis of the free drug, which can actually constitute a limit when the drug is tightly bound to a protein, as quite often occurs. To overcome this limitation, there has been continuing research to find better, faster, and more convenient approaches to the analysis of drug–protein binding.[17–20] The QCM biosensor has been recognized as a powerful implement in the monitoring of biomolecular interactions with the advantages over classical biochemical techniques of no labeling, real-time, and noninvasive measurements.[21–23] Although the QCM biosensor will not supplant high-throughput array technologies for screening, it provides a realistic possibility of low-throughput arrays and is quite useful in secondary screening situations.[24] But in this area, the QCM biosensor has not yet been fully exploited. In our previous study, we proposed a novel screening strategy based on the QCM biosensor (see Figure 1).[25] In this study, GAS was immobilized on the QCM sensor chip using an appropriate immobilization procedure and the pooled proteins were screened rapidly to determine the specific receptor. Since the binding interactions of various proteins with immobilized drug ligands were studied under similar conditions (flow rate, temperature, concentration) and on the same

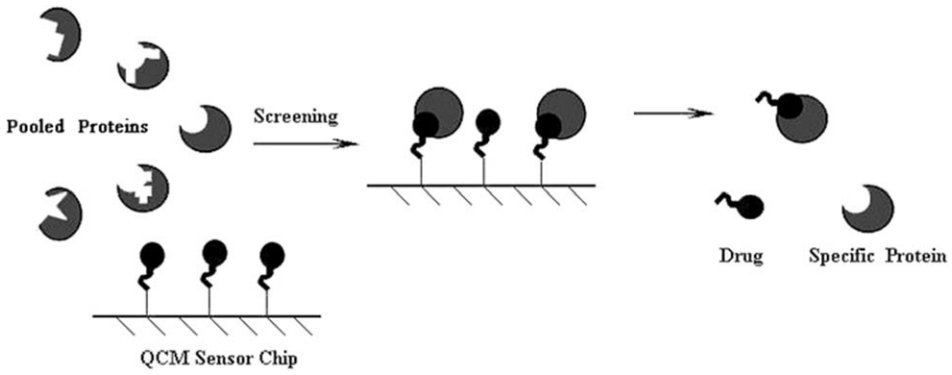

Figure 1. The strategy for rapid screen analysis of drug–protein interactions using the QCM biosensor. The drug ligand was immobilized on the QCM sensor chip for screening out specific protein.

 © 2006 Wiley-VCH Verlag GmbH & Co. KGaA, Weinheim

sensor chip, their kinetic binding curves could be compared directly to screen out the specific drug–protein interaction.

Immobilization of GAS on the QCM sensor chip: Gold surfaces can be functionalized by using a self-assembled monolayer of thio compounds. Here, dithiothreitol was chosen as the functional reagent to modify the gold electrode of piezoelectric crystal.[26,27] The sulfhydryl groups were readily activated by ethanediol diglycidyl ether under weak basic conditions and the crystal surfaces were modified with epoxide groups. GAS was then bound directly to the epoxide groups on the modified surfaces. The structures of the biorecognition layers of the two sensors, the GAS-immobilized and blank sensors, are depicted in Scheme 1. To evaluate the immobilization progress, the resonance frequencies of the dried crystals were determined after all reaction steps and the amount of bound material was determined according to the Sauerbray equation,[28] $1\ \mu g \approx 457\ Hz$ over the linear range of 0.01–25.0 μg. It was calculated that about 2.12 nmol of GAS was immobilized on each crystal surface (0.041 nmol GAS mm^{-2} gold electrode area).

The immobilization of GAS on the QCM sensor chip has two significant advantages. First, the gold electrode surfaces were covered with a self-assembled layer of dithiothreitol, which provides a hydrophilic environment suitable for most biomolecular interactions and a chemical handle for stable coupling immobilization. The free and rich hydroxy groups of the dithiothreitol can form an effective hydrophilic layer to reduce considerably the possibility of the nonspecific adsorption of protein on the gold surface. Secondly, the bis-oxirane, 1,4-butanediol diglycidyl ether, can provide not only active epoxide groups for the coupling of ligands, but also an appropriate spacer. This long spacer or arm is of great importance in biomolecular interactions. It facilitates the interactions between the small ligands immobilized on the gold surfaces and large proteins by alleviating steric hindrance.[29,30]

QCM-detected specific interaction of GAS with Fg: The QCM biosensor integrated with a FIA system is a convenient and valuable tool for real-time monitoring of the interactions. The rapid screening analysis results are shown in Figure 2. The frequency decreased by about 170 Hz when human Fg was injected into the flow-through cell. The frequency did not return to the initial level by rinsing with the loading buffer solution. This result confirmed that a strong specific interaction between Fg and immobilized GAS can occur under physiological ionic conditions. In addition, the frequency also decreased a little (by about 30 Hz) when human IgG was injected, indicating a weaker specific binding of human IgG to GAS. For other proteins, the frequencies all recovered to the baseline value on rinsing with loading buffers, indicating clearly that there was no nonspecific adsorption of these proteins by the modified sensor chip under physiological ionic conditions. As the residual epoxide groups' reacting sites have been blocked and as the gold surfaces were hydrophilic, the nonspecific adsorption of these hydrophobic proteins on the gold surfaces was almost impossible.[26]

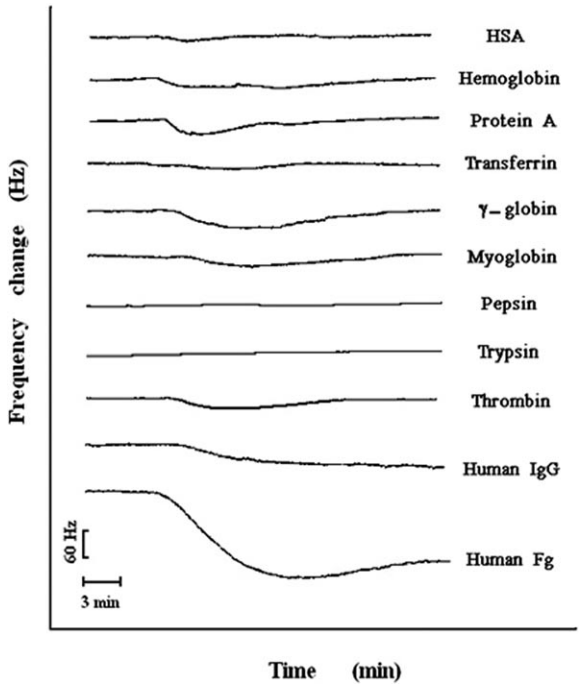

Figure 2. Rapid screen analysis of the interactions between the GAS-immobilized sensor and various proteins in solution (1 $\mu g\,\mu L^{-1}$).

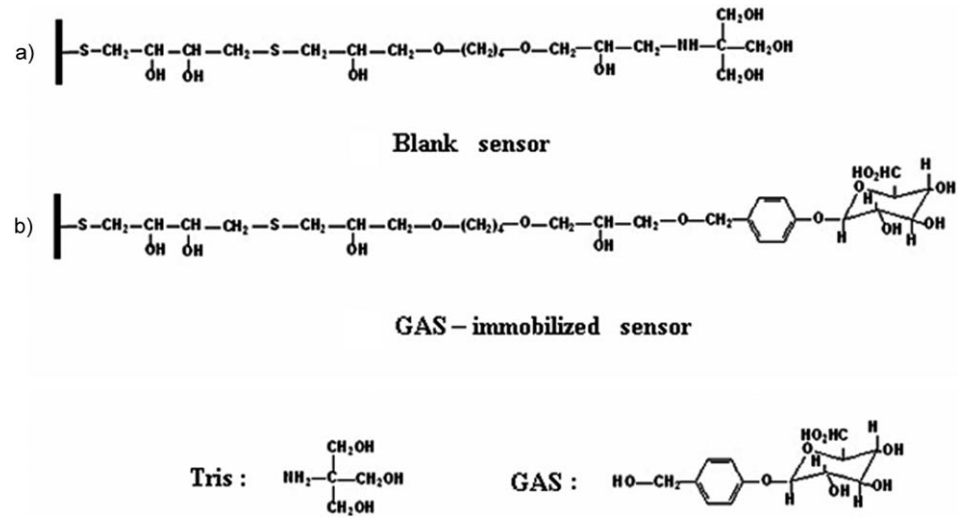

Scheme 1. The structure of biorecognition layers of two modified sensors: a) the blank sensor; b) the GAS-immobilized sensor.

 © 2006 Wiley-VCH Verlag GmbH & Co. KGaA, Weinheim

To investigate the effect of the matrix on the interaction between Fg and the immobilized GAS, the blank sensor was also placed in the flow-through cell. Then, 200 μL of Fg (1 μg μL^{-1}) was injected into the fluid system. The result was compared with the one obtained with the GAS-modified sensor (shown in Figure 3). It can be seen from Figure 3 that the blank sensor showed no binding with Fg, indicating that the matrix did not interact with Fg.

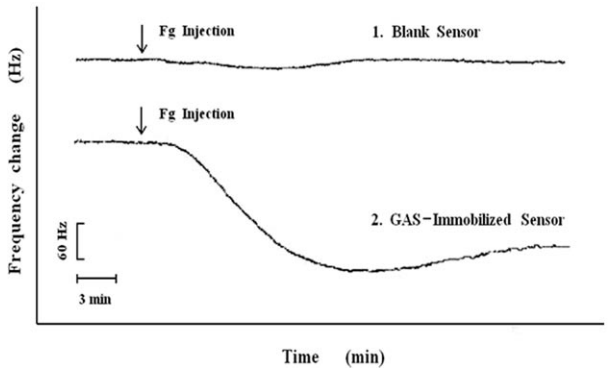

Figure 3. Interactions of human Fg with a) the blank sensor and b) The GAS-immobilized sensor.

For repeated use of the sensor, it is important to regenerate the sensor. Hence, the efficiencies of various regeneration reagents [solutions of 2 M NaCl, glycine·HCl (100 mM, pH 2.0), 10 mM HCl, and 10 mM NaOH] in removing adsorbed Fg and maintaining sensor sensitivity were compared. The 2 M NaCl solution was chosen as the best one and a typical binding and regeneration sensorgram was obtained and is shown in Figure 4. A significant decrease in frequency can be seen after 1 μg μL^{-1} of Fg was injected into the flow cell. The frequency decreased by about 170 Hz and reached equilibrium within approximately 8 min. On rinsing with the loading buffer, the frequency increased a little, indicating dissociation of the adsorbed Fg, but the frequency did not return to the initial baseline. When the 2 M NaCl solution was injected, the specifically bound Fg molecules were released and washed out in less than 20 min. The frequency recovered to the initial level. To verify the reproducibility of this experiment, 1 μg μL^{-1} of Fg was chosen and tested five times. The relative standard deviation (RSD) of the frequency shift (Δf) was calculated to be 2.3% ($n=5$), indicating that this regeneration procedure was quite reproducible.

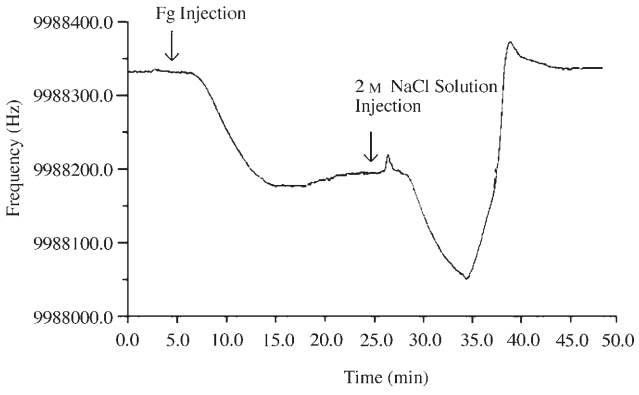

Figure 4. Typical binding and regeneration QCM sensorgram. A 2 M NaCl solution (pH 7.4) was used as the regeneration reagent.

Kinetics: Since the QCM is a continuous, real-time detector, it is possible to assess the kinetics of the interactions. Owing to steric reasons, it was assumed that only one binding site of the Fg molecule interacts with the immobilized GAS.[31,32] That is to say, the interaction between Fg and the immobilized GAS fits a 1:1 binding model and can properly be assumed to follow pseudo-first-order kinetics. For the reversible interaction, A + B⇄AB, the rate of formation of the product AB at time t may be written as Equation (1), where k_{ass} is the association rate constant and k_{diss} the dissociation rate constant. After some reaction time t, $[B]=[B]_0-[AB]$. Substituting into Equation (1) gives Equation (2), where $[B]_0$ is the concentration of B at $t=0$.

$$\frac{d[AB]}{dt} = k_{ass}[A][B]-k_{diss}[AB] \quad (1)$$

$$\frac{d[AB]}{dt} = k_{ass}[A]([B]_0-[AB])-k_{diss}[AB] \quad (2)$$

The rate of dissociation of the formed complexes, AB, is described by Equation (3).

$$\frac{d[AB]}{dt} = -k_{diss}[AB] \quad (3)$$

Considering the Sauerbray equation (the decrease in frequency F is directly proportional to the attached mass)[28] and by using F_{max} as the frequency change after complete saturation of the surface of the crystal with A, the concentration of free B is proportional to $(F_{max}-F)$ and the concentration of complex AB is proportional to F. Equation (2) and Equation (3) can thus be expressed, respectively, as Equation () and Equation (5), where C is the concentration of the free A, which is constant in a continuously flowing solution.

$$\frac{dF}{dt} = k_{ass}C(F_{max}-F)-k_{diss}F \quad (4)$$

$$\frac{dF}{dt} = -k_{diss}F \quad (5)$$

Equation (4) and Equation (5) can be integrated to give Equation (6) for the association progress and Equation (7) for the dissociation progress, where ΔF is the frequency change and C is the concentration of the free protein, which is constant in a continuously flowing solution, ΔF_{max} is the frequency change after complete saturation of the surface of the crystal with protein, t is time, t_0 is the time at the start of the reaction, and F_0 is the frequency at t_0.[33,34]

 © 2006 Wiley-VCH Verlag GmbH & Co. KGaA, Weinheim

$$\Delta F = -\frac{k_{ass} C \Delta F_{max}}{k_{ass} C + k_{diss}} [e^{-(k_{ass}+k_{diss})} - 1] \quad (6)$$

$$\Delta F = -\Delta F_0 e^{-k_{diss}(t-t_0)} \quad (7)$$

The dissociation equilibrium constant (K_D) was calculated as $K_D = k_{diss}/k_{ass}$. The in-house kinetic analysis software based on a genetic algorithm[15,25,27] was used to evaluate the results and extract kinetic data. The programs involve the following procedure: creation of population, evaluation of cost, mate selection, reproduction, and mutation. By using the procedures of mate selection, reproduction, and mutation, a new population is created and the whole circle is repeated until a proper stop criterion is fulfilled. The cost function is given by Equation (8), where y_i are the experimental data, $f(y_i,a_i)$ is the function chosen as the model, and a_i are the model parameters. The quality of the fitted data was evaluated by comparison between calculated and experimental curves and by the magnitude of χ^2.

$$\chi^2 = \frac{1}{n} \sum_{i=1}^{n} \{y_i - f(y_i,a_i)\}^2 \quad (8)$$

To obtain affinity constants, the binding and dissociation of various concentrations of Fg with the immobilized GAS were measured and recorded as sensorgrams. The results are shown in Figure 5 with the individual curves obtained shifted vertically for graphic display. The concentrations of the Fg solutions ($\mu g\,\mu L^{-1}$) are indicated next to the respective curves. The sensorgram data were fitted to Equation (6) for the "on" rate constant and to Equation (7) for the "off" rate constant. The equilibrium constant (K_D) was then determined as a ratio of k_{diss}/k_{ass}. The magnitude of χ^2 and a comparison between calculated and experimental curves were used to evaluate the quality of the fitted data. Examples of curve fitting to frequency change data for the determination of k_{ass} and k_{diss} are shown in Figure 6. The data for the adsorption and desorption process fit well when comparing the calculated and experimental curves. The results of the kinetic analyses of the interaction between immobilized GAS and Fg at various concentrations are summarized in Table 1. From Table 1, the K_D value for Fg was obtained as $(1.94 \pm 0.024) \times 10^{-6}$ M. The RSD of K_D was 1.24%, which implies that each sensorgram can provide information on the kinetic constant with acceptable precision.

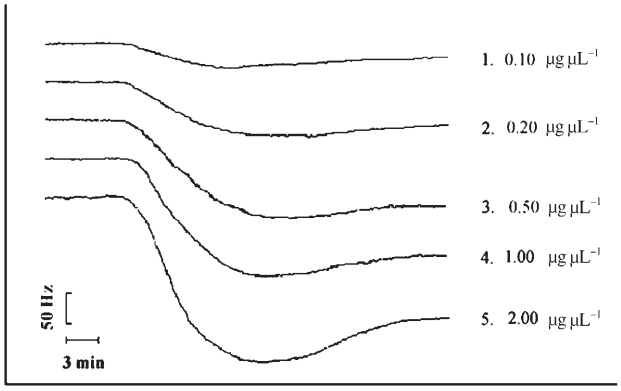

Figure 5. The individual binding curves for several concentrations of Fg with immobilized GAS.

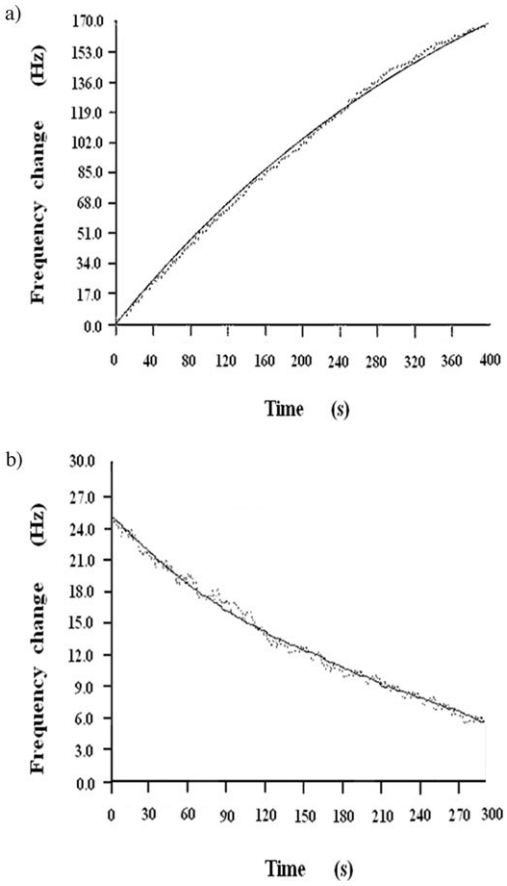

Figure 6. Curve fitting (solid lines) to frequency change data (dotted line) for the determination of k_{ass} and k_{diss}. a) Frequency modulation in Hz due to specific adsorption of Fg ($1\ \mu g\,\mu L^{-1}$) on the quartz crystal coated with GAS; b) frequency modulation in Hz due to specific desorption of Fg from the quartz crystal coated with GAS.

Table 1. Kinetic and affinity data from the QCM analysis of the interaction between Fg and immobilized GAS.

Entry	Concentration [$\mu g\,\mu L^{-1}$]	k_{ass} [$M^{-1}s^{-1}$]	$\chi^{2[a]}$ [$10^{-4}\ s^{-1}$]	k_{diss} [10^{-6} M]	$\chi^{2[b]}$	K_D
1	0.1	472	1.02	9.12	2.1	1.93
2	0.2	483	0.95	9.24	2.2	1.91
3	0.5	486	0.96	9.48	1.7	1.95
5	1.0	491	0.93	9.58	1.8	1.97
4	2.0	496	0.88	9.71	1.6	1.96

© 2006 Wiley-VCH Verlag GmbH & Co. KGaA, Weinheim

To calculate K_D, another simple approach could also be utilized. When the rates of association and dissociation reactions balance ($\frac{d[AB]}{dt}=0$ or $\frac{dF}{dt}=0$), an equilibrium characterized by the frequency change (F_{eq}) is obtained. Equation (4) can then be expressed as Equation (9) and then transformed to Equation (10).

$$K_{ass}C(F_{max}-F_{eq})-k_{diss}F_{eq}=0 \quad (9)$$

$$F_{eq}/C=1/K_DF_{max}-1/K_D \quad (10)$$

By plotting F_{eq}/C values versus the corresponding F_{eq} values, both K_D and F_{max} can be calculated by linear regression. A straight line characterized by a slope SL and intercept INT can be obtained from Equation (10). The parameters SL and INT are related to the equilibrium constant (K_D) by Equation (11) and Equation (12).

$$SL=-1/K_D \quad (11)$$

$$INT=1/K_DF_{max} \quad (12)$$

Based on this approach, K_D and F_{max} were quickly obtained from Figure 7. The correlation coefficient (r) was equal to 0.998, with $K_D=(1.82\pm0.04)\times10^{-6}$ M and $F_{max}=274\pm12$ Hz.

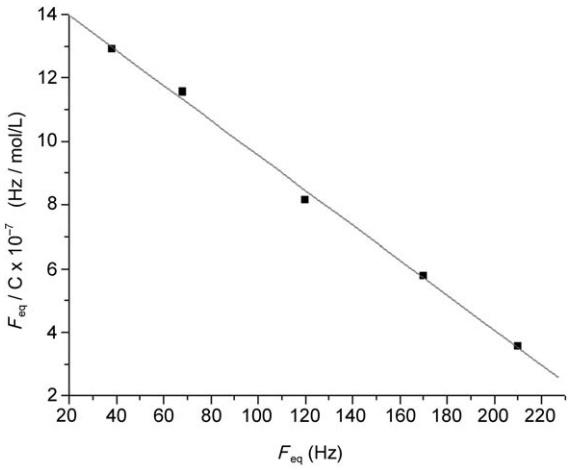

Figure 7. Values of F_{eq}/C plotted versus the corresponding F_{eq} values.

The value of K_D obtained for human IgG is close to the values shown in Table 1. This is quite a simple and convenient approach to obtaining K_D. In view of the lower K_D value, it can be deduced that the in vitro binding of GAS to Fg is strong under physiological ionic conditions.

Anticoagulant animal experiments: Although the identification of in vitro binding parameters can provide very useful quantitative or qualitative information for a given drug, only combined in vitro and in vivo data can give a complex picture of the impact of binding on its overall pharmacokinetic profile.[35] Animal models are often used in protein binding studies and the results obtained are then extrapolated to humans. To investigate whether the strong interaction with GAS could influence the coagulant function of Fg, different doses of GAS were injected into rats through their tail veins and classical clotting tests, such as CT, Fg content, KPTT, and PT, were performed in vivo. The results obtained are summarized in Table 2. The data show that GAS can prolong the CT and decrease the Fg content in a dose-dependent manner. At a dose of 30 mg kg^{-1}, GAS increased the coagulant time from 186.2 ± 14.6 s (control, $n=10$) to 206.7 ± 16.1 s ($n=10$, $p<0.01$) and decreased the Fg content from 11.43 ± 0.43 g L^{-1} (control, $n=10$) to 11.05 ± 0.51 g L^{-1} ($n=10$, $p<0.05$). The increase in the CT and decrease in Fg content by the presence of GAS are significant; they indicate that GAS has anticoagulant activity and that the strong interaction between Fg and GAS plays an important role in the expression of anticoagulant activity. Apparently, the in vivo binding of GAS can influence the normal function of Fg significantly. To further ascertain the effects of GAS on the intrinsic and extrinsic coagulation pathway, the KPTT and PT were also determined (shown in Table 2). There were no statistically significant differences in the KPTT and PT between the control group and GAS at any dosage. The KPTT determines the interference with the intrinsic coagulation pathway and the PT with the extrinsic coagulation pathway. GAS had no effect on the KPTT and PT, suggesting that its anticoagulant activity is not related to intrinsic and extrinsic coagulation factors.[36] It appears that GAS interferes rather with the final stage of the blood coagulant cascade than with the intrinsic or extrinsic coagulant cascade. That is to say, the anticoagulation activity by GAS is mainly due to its strong binding to Fg, thereby inhibiting its conversion to the fibrin clot in the final stage of the blood coagulant cascade.[37]

Table 2. In vivo effect of GAS on the coagulant system of rats.[a]

Group	Dose [mg kg^{-1}]	CT [s]	Fg content [g L^{-1}]	KPTT [s]	PT [s]
control	–	186.2 ± 14.6	11.43 ± 0.43	22.6 ± 0.9	14.6 ± 0.5
GAS	7.5	185.5 ± 17.7	11.28 ± 0.39	22.7 ± 0.8	14.5 ± 0.3
GAS	15	194.9 ± 12.3	11.13 ± 0.48	22.2 ± 0.9	14.8 ± 0.4
GAS	30	206.7 ± 16.1[a]	11.05 ± 0.51[b]	22.3 ± 1.0	14.5 ± 0.4

[a] Mean ± S.D., $n=10$. [b] Compared with the control group, $P<0.01$. [c] Compared with the control group, $P<0.05$.

Molecular modeling: To gain a better understanding of the molecular basis for the specific interaction between GAS and Fg, a molecular docking method was used to construct the binding models of GAS with Fg and to predict their binding affinities. Here, the binding free energies are predicted to be −33.8 KJ mol^{-1} for an "a" hole and −34.4 KJ mol^{-1} for a "b" hole. Thus, GAS binds to the inherent polymerization sites, the "a" and "b" holes, on the Fg molecule with similar binding free energies of about −34 kJ mol^{-1}. The contributions to the bindings are 10% for van der Waals interactions, 48% for hydrogen-bonding

 © 2006 Wiley-VCH Verlag GmbH & Co. KGaA, Weinheim

energy, and 42% for hydrophobic energy. For the "b" hole, the contributions of different energies were predicted to be 14% for van der Waals interactions, 45% for hydrogen-bonding energy, and 41% for hydrophobic energy. It can be seen that hydrophobic interactions and hydrogen bonds play key roles in GAS–Fg binding.

The binding mode of GAS in the "a" and "b" holes is displayed in Figure 8a and 8b, respectively. The 3D models provide a good explanation for the strong interaction from a structural viewpoint. The GAS ligand can roughly be divided into two parts, that is, the hydrophobic benzyl part and the hydrophilic saccharide part (shown in the 2D formula in Figure 8). For the "a" hole, the side-chains of residues Tyr363, Phe322, and Lys338 are mainly involved in the hydrophobic interaction with the benzyl part of GAS and the side-chains of residues Asp330, His340, and Asp364 are involved in the hydrogen-bonding interaction with the saccharide part of GAS. Similarly, for the "b" hole, the side-chains of residues Met367, Leu360, and Arg406 are mainly involved in the hydrophobic interaction with the benzyl part of GAS and the side-chains of residues Asp398, His408, and Asp432 are involved in the hydrogen-bonding interaction with the saccharide part of GAS.

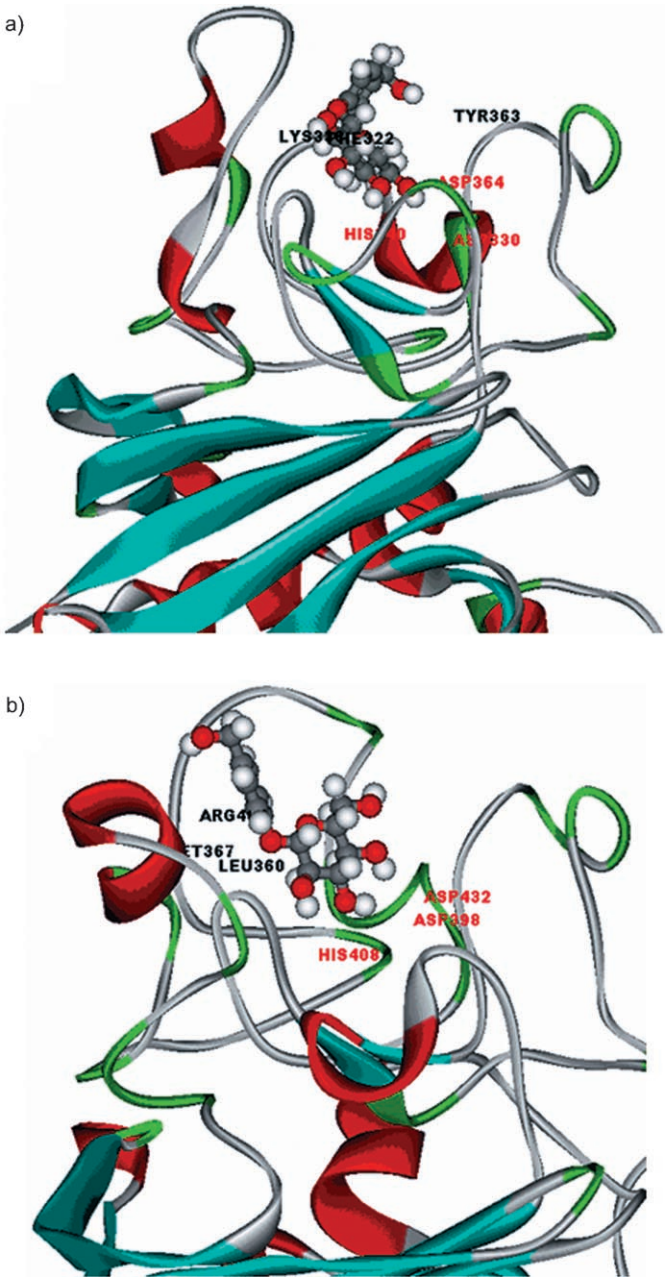

Figure 8. The binding modes of GAS with Fg in a) an "a" hole and b) a "b" hole.

It is also interesting to compare the binding modes of GAS with the binding modes of the natural ligands Gly-Pro-Arg-Pro and Gly-His-Arg-Pro. The superimpositions of the docking poses of GAS and the natural ligands are shown in Figure 9a and 8b. The binding modes of GAS and the natural ligands are quite similar: in the "a" hole, the hydrophobic part of the side chain of Arg and the Pro4 of the peptide correspond with the benzyl part of GAS and are bound to the receptor through a hydrophobic interaction. The hydro-

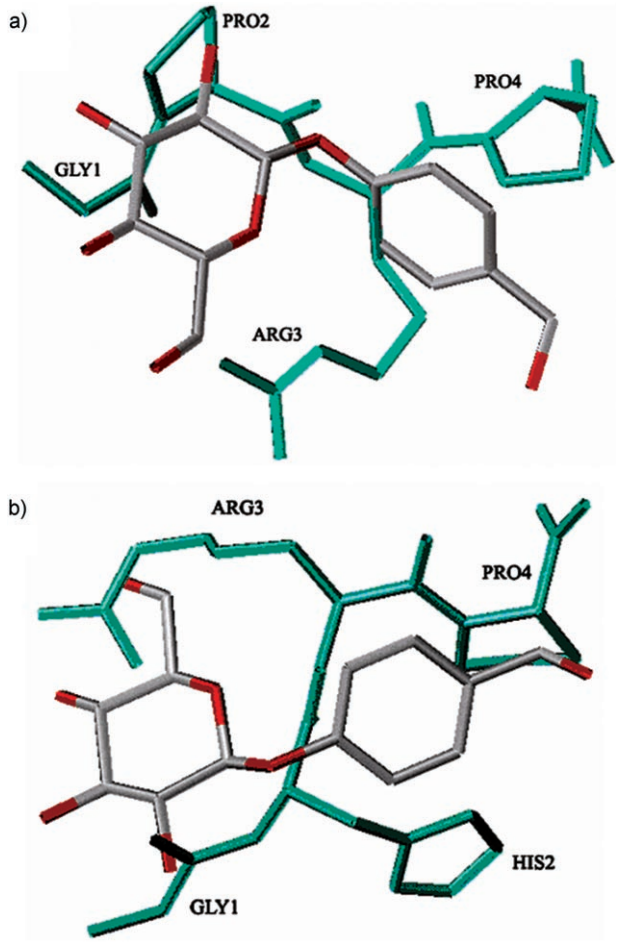

Figure 9. The superimposition of the docking poses of GAS (colored by atom types) and natural ligands (colored in blue). a) The superimposition of the docking poses of GAS and the natural ligand (Gly-Pro-Arg-Pro) in the "a" hole; b) the superimposition of the docking poses of GAS and the natural ligand Gly-His-Arg-Pro in the "b" hole.

 © 2006 Wiley-VCH Verlag GmbH & Co. KGaA, Weinheim

philic part of the side chain of Arg and the main chains of Gly and Pro2 of the peptide correspond with the saccharide part of GAS and form a hydrogen-bond network with the receptor; in the "b" hole, the side chains of His and Pro of the peptide correspond with the benzyl part of GAS and bind to the receptor mainly by hydrophobic interactions. The terminal part of Gly and the side chain of Arg of the peptide correspond with the saccharide part of GAS and form a hydrogen-bond network with the receptor. These superimpositions imply that the predicted binding modes of GAS in the "a" and "b" holes of Fg are both reasonable.

On the basis of the foregoing results and discussion, one can suggest that a possible anticoagulation mechanism of GAS mainly involves its strong interference with the knob-to-hole interactions between fibrin molecules, thereby effectively inhibiting the formation of fibrin clots.[38,39]

Conclusion

This is the first demonstration of the anticoagulant activity of GAS, suggesting its possible use as a promising anticoagulant lead compound. The results of this study provide valuable insights into the structural and functional basis of the GAS–Fg interaction and have laid a foundation for the research into the anticoagulant mechanism of GAS and the application of this novel anticoagulant. Moreover, this work also demonstrates that the QCM biosensor is a suitable technique for the rapid and sensitive screening of drug–protein interactions. The screening approach based on the QCM biosensor is expected to be a promising way of discovering the special biological activities of some other new drugs.

Experimental Section

Materials: GAS was the chemical control reagent supplied by the National Institute for the Control of Pharmaceutical and Biological Products (Beijing, China). DL-Dithiothreitol (DTT), human serum albumin (HSA), hemoglobin, protein A, transferrin, γ-globin, myoglobin, pepsin, trypsin, thrombin, human IgG, and human Fg were all purchased from Sigma (St. Louis, MO). 1,4-Butanediol diglycidyl ether and sodium borohydride were from Aldrich (St. Louis, MO). All other chemicals were analytical reagent grade. Unless otherwise noted, all the reagents were made up in a 10 mM phosphate buffered solution (PBS) containing 150 mM NaCl at pH 7.4. Prior to use, all solutions prepared were filtered (0.45 μm).

The QCM sensors employed were 10 MHz AT-cut quartz crystals (14 mm diameter) with gold electrodes (8 mm diameter, geometric area: 50.2 $mm^2 \times 2$) on both sides purchased from Beijing 707 Factory (Beijing, china). The crystals were polished to a surface roughness of less than 5 μm, which produced a mirror-like finish on the gold electrodes.

Male Wistar rats (body weight 195–200 g) were obtained from the Institute of Laboratory Animals, Chinese Academy of Medical Sciences (Beijing, China). Fg content, KPTT, and PT kits were purchased from Shanghai Sun Biological Products Co. (Shanghai, China).

Immobilization of GAS on the QCM chip: First, the gold electrodes on the quartz crystal were cleaned as described previously.[15] Then the freshly cleaned gold surfaces were immersed in a 20 mM ethanol solution of DTT. The unstirred solution was kept at room temperature in the dark for 24 h. The crystal was then washed with ethanol and doubly distilled water and sonicated for 10 min in ethanol to remove excess thiol. The modified crystal was immersed in a solution consisting of ethanediol diglycidyl ether (1 mL), 0.1 M Na_2CO_3 buffer solution (4 mL, pH 8.5) and sodium borohydride (8 mg). The reactions were performed at 30 °C for 4 h and stopped by washing the surfaces with a large volume of water. The prepared crystal was immersed for 4 h in a basic solution containing GAS (10 mg) in a 0.1 M Na_2CO_3 buffered solution (5 mL, pH 11.0) and the reaction temperature was kept at 40 °C. Finally, Tris-HCl (5 mL, 1.0 M, pH 8.5) was used as a blocking agent and applied for 30 min to block the residual reacting sites. A blank sensor was also prepared according to the above immobilization procedure but without following the GAS ligand coupling procedure.

QCM biosensor kinetic analysis: An in-house QCM-FIA system with kinetic analysis software based on a genetic algorithm (GA), as previously described in detail[15,27] was used for the real-time kinetic analysis of the interaction between immobilized GAS and proteins in solution. The freshly modified quartz crystal was mounted in the flow-through cell and continuously rinsed with the loading solution (10 mM PBS containing 150 mM NaCl, pH 7.4) until the frequency had stabilized under the flow conditions (60 $\mu L\,min^{-1}$). By means of an injection valve, various protein solutions (200 μL) were injected into the fluid system. The permanent frequency shift versus time curves were recorded and the binding process was monitored in real time. After one binding measurement, a 2 M NaCl solution (600 μL, pH 7.4, PBS buffer) was injected into the system with the injection valve to dissociate the bound protein and free binding sites in the receptor layer for the next binding measurement. The experimental sensorgram data were analyzed using our in-house kinetic analysis software based on a GA to obtain the binding constants rapidly.

Anticoagulant animal experiments: The anticoagulant activity of GAS was evaluated by classical coagulation assays.[40,41] The study was approved by Xiyuan Hospital, Chinese Academy of Medical Sciences (Beijing, China). Forty rats were randomly divided into four groups ($n = 10$ in each group): a control group treated with normal saline and three GAS groups treated with different doses of GAS (7.5, 15, and 30 $mg\,kg^{-1}$). Normal saline or GAS was injected into the tail vein of the rats at a volume of 3 $mL\,kg^{-1}$ once everyday. On the third day, animals were anaesthetized by celiac injection of 1% sodium pentobarbital at a volume of 3 $mL\,kg^{-1}$ after 15 min when administration was finished. Blood samples were then collected from abdominal aorta. At the same time as the sampling, the CT was determined by the capillary tube method. The blood obtained was anticoagulated with 3.8% sodium citrate (9:1, v/v) and centrifuged at 1500 g for 10 min to obtain platelet-poor plasma.[42] Then the Fg content, KPTT, and PT were measured by a ThromboScreen 400C four channels coagulometer (Fisher Scientific International Inc., Pittsburgh, PA). The results have been presented as the mean ± standard deviation (mean ± S.D.). The significance of the differences between the groups was determined by Student's *t*-test and $P < 0.05$ was considered significant.[43]

Molecular docking: The molecular model of GAS was constructed by using the SYBYL 6.91 program, optimized with the TRIPOS 5.5 force field and stored in the Mol2 file format.[44] Then it was flexibly docked into the binding pockets of human Fg (taken from the protein data bank, PDB code 1LTJ)[45] using the Pose-Sensitive Inclined Dock (PSI-DOCK) 1.0 program.[46] The PSI-DOCK 1.0 program is highly efficient in identifying the experimental binding pose. For a test data set of 194 complexes, PSI-DOCK 1.0 achieved a 74% success rate. In 1LTJ, there are two natural peptide ligands (Gly-Pro-Arg-Pro and Gly-His-Arg-Pro) binding to two similar binding pockets on chain C (the "a" hole) and chain B (the "b" hole) of Fg, respectively. We removed the natural peptide ligands from the binding pockets and docked GAS in them. For each binding pocket, the PSI-DOCK docking program was run 10 times and the lowest binding energy pose of the ligand was selected as the final docking pose. The final binding free energies were calculated by using the empirical SCORE 3.0 function embedded in the PSI-DOCK program. The SCORE 3.0 function includes terms to account for van der Waals contacts, metal–ligand bonding, hydrogen bonding, desolvation effects, and entropy effects upon binding. The PSI-DOCK program can predict the

 © 2006 Wiley-VCH Verlag GmbH & Co. KGaA, Weinheim

ligand–protein binding free energy with a high degree of accuracy of a standard error of 7.96 kJ mol^{-1}.[46]

Acknowledgements

We thank Prof. Huiwan Han of Tsing Hua University for helpful discussions. We are also grateful to the National Natural Science Foundation of China (No. 20405001 and No. 20335010) and the Postdoctoral Science Foundation of China (No. 2004035245) for financial support of this work.

[1] C. Sotriffer, G. Klebe, *Il Farmaco* **2002**, *57*, 243–251.
[2] U. Kragh-Hansen, *Pharmacol. Rev.* **1981**, *33*, 17–53.
[3] A. Chattopadhyay, T. Tian, L. Kortum, D. S. Hage, *J. Chromatogr. B* **1998**, *715*, 183–190.
[4] R. F. Doolittle, *Annu. Rev. Biochem.* **1984**, *53*, 195–229.
[5] V. C. Yee, K. P. Pratt, H. C. F. Côté, I. L. Trong, D. W. Chung, E. W. Davie, R. E. Stenkamp, D. C. Teller, *Structure* **1997**, *5*, 125–138.
[6] S. A. Olexa, A. Z. Budzynski, *Proc. Natl. Acad. Sci. USA* **1980**, *77*, 1374–1378.
[7] S. Yakovlev, E. Makogonenko, N. Kurochkina, W. Nieuwenhuizen, K. Ingham, L. Medved, *Biochemistry* **2000**, *39*, 15730–15741.
[8] K. L. Marchin, C. L. Berrie, *Langmuir* **2003**, *19*, 9883–9888.
[9] B. M. Coull, L. S. Williams, J. F. Meschia, D. Heitzman, S. Chaturvedi, K. C. Johnston, S. Starkman, L. B. Morgenstern, J. L. Wilterdink, S. R. Levine, J. F. Saver, *Stroke* **2002**, *33*, 1934–1942.
[10] A. J. Chu, S. Beydoun, S. T. Mathews, J. Hoang, *Arch. Biochem. Biophys.* **2003**, *415*, 101–108.
[11] A. P. Laudano, R. F. Doolittle, *Proc. Natl. Acad. Sci. USA* **1978**, *75*, 3085–3089.
[12] Y. K. Zhao, Q. Cao, Y. Q. Xiang, Z. D. Hu, *J. Chromatogr., A* **1999**, *849*, 277–283.
[13] H. B. Li, F. Chen, *J. Chromatogr. A* **2004**, *1052*, 229–232.
[14] Y. H. Cao, X. Zhang, Y. Z. Fang, J. N. Ye, *Analyst* **2001**, *126*, 1524–1528.
[15] Y. Liu, X. Yu, R. Zhao, D. H. Shangguan, Z. Y. Bo, G. Q. Liu, *Biosens. Bioelectron.* **2003**, *18*, 1419–1427.
[16] C. Bertucci, S. Cimitan, *J. Pharm. Biomed. Anal.* **2003**, *22*, 707–714.
[17] A. Shibukawa, Y. Kuroda, T. Nakagawa, *TrAC Trends Anal. Chem.* **1999**, *19*, 549–556.
[18] R. L. Rich, Y. S. N. Day, T. A. Morton, D. Myszka, *Anal. Biochem.* **2001**, *296*, 197–207.
[19] B. P. Kamat, J. Seetharamappa, *J. Pharm. Biomed. Anal.* **2004**, *23*, 655–664.
[20] M. A. Cooper, *Anal. Bioanal. Chem.* **2003**, *377*, 834–842.
[21] Y. Zhang, V. Telyatnikov, M. Sathe, X. Zeng, P. G. Wang, *J. Am. Chem. Soc.* **2003**, *125*, 9292–9293.
[22] X. Su, R. Robelek, Y. Wu, G. Wang, W. Knoll, *Anal. Chem.* **2004**, *76*, 489–494.
[23] H. Matsuno, H. Furusawa, Y. Okahata, *Biochemistry* **2005**, *44*, 2262–2270.
[24] B. A. Čavić, G. L. Hayward, M. Thompson, *Analyst* **1999**, *124*, 1405–1420.
[25] Y. Liu, X. L. Tang, F. Liu, K. Li, *Anal. Chem.* **2005**, *77*, 4248–4256.
[26] Y. Liu, W. Zhang, X. Yu, H. W. Zhang, R. Zhao, D. H. Shangguan, Y. Li, B. F. Shen, G. Q. Liu, *Sens. Actuators, B* **2004**, *99*, 416–424.
[27] Y. Liu, X. Yu, R. Zhao, D. H. Shangguan, Z. Y. Bo, G. Q. Liu, *Biosens. Bioelectron.* **2003**, *19*, 9–19.
[28] G. Z. Sauerbrey, *Phys.* **1959**, 155, 206–222.
[29] L. Sundberg, J. Porath, *J. Chromatogr.* **1974**, *90*, 87–98.
[30] I. S. Park, N. Kim, *Biosens. Bioelectron.* **1998**, *13*, 1091–1097.
[31] M. J. Eddowes, *Biosensors* **1987**, *3*, 1–15.
[32] P. Skládal, M. Minunni, M. Mascini, V. Kolár, M. Fratiek, *J. Immunol. Methods* **1994**, *176*, 117–125.
[33] A. Hengerer, J. Decker, E. Prohaska, S. Hauck, C. Kõβlinger, H. Wolf, *Biosens. Bioelectron.* **1999**, *14*, 139–144.
[34] A. Hengerer, C. Kõsslinger, J. Decker, S. Hauck, I. Queitsch, H. Wolf, S. Dübel, *Biotech.* **1999**, *26*, 956–964.
[35] J. Oravcová, B. Böhs, W. Lindner, *J. Chromatogr. B* **1996**, *677*, 1–28.
[36] S. Alban, G. Franz, *Biomacromolecules* **2001**, *2*, 354–361.
[37] E. D. Cera, *Trends Cardiovasc. Med.* **1998**, *8*, 340–350.
[38] Y. Tamada, M. Murata, T. Hayashi, K. Goto, *Biomaterials* **2002**, *23*, 1375–1382.
[39] M. Kyogashima, T. Sakai, J. Onaya, A. Hara, *Glycoconjugate J.* **2001**, *18*, 245–251.
[40] M. Sakai, H. Ohteki, Y. Narita, K. Naitoh, M. Natsuaki, T. Itoh, *J. Cardiovasc. Surg.* **1999**, *40*, 187–194.
[41] H. Türk, R. Haag, S. Alban, *Bioconjugate Chem.* **2004**, *15*, 162–167.
[42] Y. Tamada, M. Murata, K. Makino, Y. Yoshinori, T. Yoshida, T. Hayashi, *Biomaterials* **1998**, *19*, 745–750.
[43] A. J. Chu, S. Beydoun, S. T. Mathews, J. Hoang, *Arch. Biochem. Biophys.* **2003**, *415*, 101–108.
[44] SYBYL, version 6.91, Tripos Associates, St. Louis, MO, **2004**.
[45] M. S. Kostelansky, L. Betts, O. V. Gorkun, S. T. Lord, *Biochemistry* **2002**, *41*, 12124–12132.
[46] J. F. Pei, Q. Wang, Z. M. Liu, Q. L. Li, K. Yang, L. H. Lai, *Protein J.* **2006**, *62*, 934–946.

Received: April 18, 2006
Published online: July 18, 2006

 © 2006 Wiley-VCH Verlag GmbH & Co. KGaA, Weinheim